Two-tensor streamline tractography through white matter intra-voxel fiber crossings: assessed by fMRI

Arish A.Qazi[1,2], Gordon Kindlmann[1], Lauren O'Donnell[1], Sharon Peled[1], Alireza Radmanesh[1], Stephen Whalen[1], Alexandra J.Golby[1], Carl-Fredrik Westin[1]
[1]Harvard Medical School, Boston MA, USA
[2]University of Copenhagen, Denmark
qazi@bwh.harvard.edu

Abstract

An inherent drawback of the traditional diffusion tensor model is its limited ability to provide detailed information about multidirectional fiber architecture within a voxel. This leads to erroneous fiber tractography results in locations where fiber bundles cross each other. In this paper, we present a deterministic two-tensor eXtended Streamline Tractography (XST) technique, which successfully traces through regions of crossing fibers. The method has been evaluated on simulated and in-vivo human brain data, and compared with the traditional single tensor, and a probabilistic tractography technique. By tracing the corticospinal tract we demonstrate that when compared to the two methods, our technique can accurately identify fiber bundles known to be consistent with anatomy. When compared to the dense connectivity maps generated by probabilistic tractography, the method is computationally efficient and generates discrete geometric pathways that are simple to visualize and clinically useful.

1. Introduction

Diffusion-weighted MRI (DWI) provides a unique way to probe tissue microstructure by characterizing the random motion of water molecules within the tissue. Diffusion tensor imaging, an extension of DWI, allows visualization of white matter fiber orientations by finding the preferred direction of water diffusion [1]. The reconstruction of fiber bundles is usually carried out by line propagation or streamline techniques using the principal eigenvector of the diffusion tensor [1, 2].

Fiber tractography, however, is difficult in places where fiber bundles intersect each other. For example, fibers in the upper-extremity motor cortex of the brain curve inferiorly and medially, and intersect the superior longitudinal fasciculus (SLF), which tracks anteroposteriorly through the corona radiate, and the centrum semiovale. Due to the orientational heterogeneity in such locations the principal eigenvector does not correspond to the fiber direction [3], and thus the traditional diffusion tensor model fails to estimate the correct fiber orientations.

An inherent drawback of the single diffusion tensor model is its limited ability to provide detailed information about multidirectional fiber architecture within a voxel. This limitation of the traditional tensor model has lead to the development of new acquisition techniques along with more complex models of diffusion. One strategy to characterize the underlying complex fiber architecture is to quantify the diffusion function using the Fourier relationship first observed by Stejskal and Tanner [4], between the diffusion function and the diffusion signal attenuation in q-space [5]. Q-space imaging methods [6] are essentially model independent; they aim at directly measuring the 3D probability diffusion function of water molecules. Inherent drawback of these methods, however, are large number of gradient directions (typically > 100), incurring long acquisition times, which make them infeasible in a clinical setting.

There have been previous works which attempt to explicitly model the complexity of the DWI formation in the presence of multiple fibers [7]. A simple model is a mixture of Gaussian densities [3, 8], which can thought of as a generalization of the single tensor model. It should be noted, however, that the constraints on the parameters of these models are non-linear; therefore the optimization is time intensive, along with the problem of robustly yielding a global minimum for the objective function. Another inherent problem is that the model has no knowledge of the actual number of fibers present in a voxel; therefore accuracy may be reduced by representing the voxel with multiple fiber orientations when it can be better represented by a single fiber.

Recently, Peled et al. introduced a constrained bi-Gaussian model for analysis of crossing fibers with fewer model parameters, utilizing the information present in the single tensor [9]. This two-tensor approach models a voxel containing two tracts as 2 cylindrical tensors (with identical eigenvalues), that lie in the plane spanned by the two largest eigenvectors of the single tensor fit. These physically realistic constraints contribute to the robustness of the fit even with a relatively small number of acquired gradient directions.

1.1. Multi-fiber Tractography

Attempts have been made to incorporate complex models of diffusion in both deterministic (streamline) [8, 10] and probabilistic techniques [11-13]. Due to the classic limitations of deterministic algorithms: such as choice of initialization, and the inability to trace accurately in regions of crossing fibers, probabilistic tractography methods have been developed as an alternative.

For some application domains, however, such as neurosurgical planning and guidance, deterministic tractography has several advantages over probabilistic tractography. First, deterministic methods are fast and may be used interactively. Second, visualization of the streamline trajectories is qualitatively similar to the expected white matter fiber tract connections; whereas visualization of connection probabilities may be harder to interpret. Instead of recognizable and discrete geometric pathways, probabilistic methods generate a dense 3D volume of potential connectivities, which cannot be easily inspected except by further visualization methods (cutting planes, projections, isosurfaces, etc.). Fig. 1 illustrates a simulation on synthetic data (details are enlisted in the next section) which shows the resultant fibers from single and two-tensor based deterministic tractography, along with their probabilistic counterpart.

Thus, the aim of this paper is to present a two-tensor deterministic tractography method that resolves some of the limitations of current tractography method. The method presented is called eXtended Streamline Tractography (XST), and is a technique based on the constrained two-tensor model proposed in [9]. In this paper, we evaluate the performance of XST based tractography by comparing the results to those obtained from traditional single tensor tractography, and the probabilistic tractography technique proposed in [12]. The methods are compared by seeding in the internal capsule, and determining whether a method successfully reconstructs major fiber bundles arising from the primary motor cortex, where the anatomical origin of the fiber bundle is determined by fMRI activation maps.

2. Methods

2.1. Background Theory

In a diffusion-weighted MRI experiment extra gradient pulses are introduced, and the amount of signal loss S_q when compared to the original signal S_0 (without diffusion weighting) is modeled by the following equation [14]:

$$S_q = S_0 e^{-b\hat{g}^t D\hat{g}} \tag{1}$$

where D is the apparent diffusion tensor (ADT). The eigenvalues of D are the apparent diffusion constants in the principal directions, $\hat{g}$ is a unit vector representing the direction of a diffusion gradient, and b is a factor describing the gradient timing and strength [15]. To estimate the tensor D, Eq. [1] is usually solved by the linear least squares method.

2.2. Two-Tensor Model

Eq. [1] describes the signal attenuation function for a single tensor model, which is described by a Gaussian function. The signal attenuation equation for a generalized two-tensor model can similarly be described by a weighted sum of two Gaussian functions:

$$S = S_0\left(fe^{-bg^t D_1 g} + (1-f)e^{-bg^t D_2 g} \right) \tag{2}$$

Eq. [2] has 13 unknowns, compared to six in the single-tensor case (six parameters for each of the two diffusion tensors D_1 and D_2 plus the fraction factor f). Given the known noise-sensitivity of the single-tensor model [16], the greater number of degrees of freedom is problematic for the two-tensor. To address this, we use the constrained two-tensor model of Peled et al. [9], with only seven degrees of freedom. The model utilizes information from the single tensor fit; it assumes that both fiber tracts are constrained in the plane spanned by the first two principal eigenvectors $(\hat{e}_1, \hat{e}_2)$. A further assumption of the model is that the apparent diffusion constants parallel and perpendicular are same for both the fiber tracts. With the single tensor fit determining 3 degrees of freedom (orientation of $\hat{e}_3$ and minor eigenvalue λ_3) the remaining free parameters are:

- *f:* fraction of the first tensor, or the weighting factor,
- ϕ_x and ϕ_y : the angles subtended in the plane by the principal directions of the two diffusion tensors and,
- λ_1: the principal eigenvalue which is assumed to be same for both the fiber tracts.

Given the above constraints the two tensors are represented in the principal frame of the single tensor fit as:

$$D_x = \begin{bmatrix} d_{x1} & d_{x3} & 0 \\ d_{x3} & d_{x2} & 0 \\ 0 & 0 & \lambda_3 \end{bmatrix}, D_y = \begin{bmatrix} d_{y1} & d_{y3} & 0 \\ d_{y3} & d_{y2} & 0 \\ 0 & 0 & \lambda_3 \end{bmatrix}$$

where

$$d_{p1} = \cos^2 \phi_p \lambda_1 + \sin^2 \phi_p \lambda_3, \, p \in \{x, y\}$$

$$d_{p2} = \sin^2 \phi_p \lambda_1 + \cos^2 \phi_p \lambda_3$$

$$d_{p3} = \cos \phi_p \sin \phi_p \left(\lambda_1 - \lambda_3 \right)$$

λ_3 is calculated from the single tensor fit. Transforming the gradients in the new coordinate system the signal attenuation equation is then represented as:

$$S_q = S_0 \left(f e^{-b \hat{G}^t D_x \hat{G}} + (1 - f) e^{-b \hat{G}^t D_y \hat{G}} \right) \quad (3)$$

In this work, Eq. [3] was solved using the Levenberg-Marquardt non-linear optimization method. As in the single tensor case, the model can be fitted to every voxel however fitting a more complex model to the data may lead to a poor estimate of the underlying fiber orientation. Thus, only planar voxels were subjected to the more complex two-tensor fit where the degree of "planarity" was determined by C_p, which is Westin's planar anisotropy index [17].

2.3. eXtended Streamline Tractography (XST)

To incorporate two principal diffusion directions we need to extend the traditional streamline method proposed in [1]. The method starts from an initial seed point, and the fibers are propagated by solving the following 3D path equation:

$$\frac{ds(t)}{dt} = r(t) \quad (4)$$

where *s*(t) is the fiber curve path position at time *t* and *r*(t) is the local tangent orientation of the path. Eq. [4] can be numerically solved by Euler or Runga-Kutta integration schemes.

To trace a continuous path in the single tensor case, the integration scheme requires repeated tensor interpolation to derive a tensor at an arbitrary position. This is usually done by a weighted sum of neighboring tensors. With two rather than one tensor per sample, however, there is correspondence ambiguity inherent in the interpolation. Between two samples (each with two tensors), there are two ways of establishing correspondence, but the combinatorics become complex with the 2x2x2 sample neighborhood for trilinear interpolation or the 4x4x4 neighborhood for tricubic interpolation. To avoid this complex correspondence problem, the diffusion weighted images (DWIs) were interpolated at each step along the estimated tract path, and for each step the two tensors were estimated from the interpolated DWIs using Eq. [3]. Thus the model-fitting here is performed after interpolation, which is in contrast to both previous work in single-tensor tractography, and in probabilistic tractography where model fitting is performed first, followed by model interpolation [12].

Although the correspondence problem is removed by performing the two-tensor model fitting after interpolation, one of the two tensors must be chosen when tracing a specific path. For this we choose the tensor whose principal eigenvector has the least deviation from the incoming path direction. For single tensor tractography, the trace stopping criterion is normally based on detecting low anisotropy, since the direction of the tensor becomes more and more uncertain when the anisotropy is reduced. In two-tensor tractography defining the stop criterion is more complex, since the methods are designed to trace through low (single-tensor) anisotropy regions. In this work, paths are terminated when linear anisotropy (as measured by C_l [17]) falls below a given threshold (typically 0.2-0.3),or when the radius of curvature becomes too small (2.3*mm*), or when the fraction of the chosen tensor component is lower than 0.1. Further, if the resultant trace-line is shorter than a predefined length (here selected to 40*mm*) it is discarded.

The trace-lines were seeded from hand-drawn regions of interest, and to ensure a dense set of paths, seed points were place at nine evenly-spaced points within each voxel. If the seed point was a crossing (according to the planer measure threshold described earlier) then two separate paths were generated from the seed point, along the two tensor components. In our implementation we used cubic interpolation [18] and fourth-order Runga-Kutta integration to solve Eq. [4].

2.4. Probabilistic Tractography

In order to better understand the merits of the developed two-tensor stream-line tractography method, it was compared to a recent probabilistic technique proposed by Behrens et al. [12]. The probabilistic method is a part of FSL (FMRIB's Software Library: http://www.fmrib.ox.ac.uk/fsl/). All the parameters for the method were same as in [12].

2.5. Synthetic Data Generation

Based on Eq. [3] two anisotropic tensors with eigenvalues 1.7, 0.2, 0.2 x 10^{-3} mm^2/s were simulated,

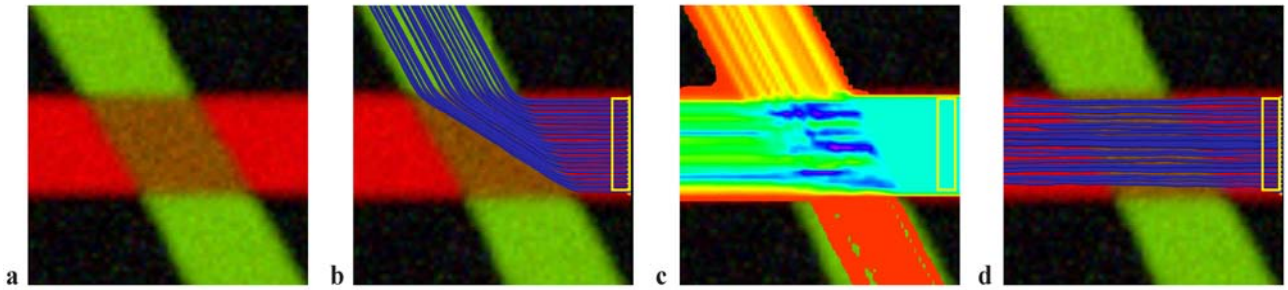

Figure 1: Simulated data. (a) The simulated 60° fiber crossing. Inside the brown region (middle), the two fibers are crossing each other. Outside the region there is one anisotropic tensor, and the direction is color-coded. (b) Single tensor tractography when seeded in the region bounded by the yellow box. (c) Connection map from Probabilistic tractography when seeded in the same region (voxels are color coded from 5000 (blue) to 4 (red) samples passing through the voxel). (d) Tractography based on XST.

corresponding to the eigenvalues in the splenium of the corpus callosum [19]. The DWI's were then estimated for each voxel of the image. The number of gradient directions was 55, with b = 1000 s/mm^2, and 5 non-diffusion-weighted images. The fraction of signal for the two tensors was kept constant at 0.5. The fibers cross at the center of the image at an angle of 60°. Outside the crossing region the tensors were anisotropic and at the border they were chosen to be isotropic. Additionally, complex Gaussian noise was added to simulate an SNR of 18, 20, and 22. Fig. 1 (a) illustrates a simulated slice with a 60° fiber crossing at an SNR of 18.

2.6. Human Brain Data

After informed consent, the subjects underwent the following MR imaging protocol on a General Electric (Milwaukee, WI), 3T Signa scanner with Excite 14.0, using an 8-channel head coil and ASSET. As a first step, a high resolution whole brain T1-weighted axial 3D SPGR (TR=7500*ms*, TE=30*ms*, matrix=256x256, FOV=25.6*cm*, FA=20°; imaging 176 slices of 1*mm* thickness) was acquired. Next, DWI was acquired with a multi-slice single shot diffusion weighted echo-planar-imaging sequence (TR=14000*ms*, TE=76.6*ms*) consisting of 55 gradient directions with a b-value of 1000 s/mm^2, and 5 baseline T2 images. The FOV was 25.6*cm*. Imaging matrix was 128x128 with a slice thickness of 2.6*mm*.

2.7. Function MRI (fMRI) activations

Whole-brain functional images were acquired using a quadrature coil with a T2*-weighted echo planar (EPI) sequence sensitive to the blood oxygen-level-dependent (BOLD) signal (TR=2000*ms*, TE=30*ms*, matrix=128x128, FOV=25.6*cm*; imaging 27 interleaved slices of 4*mm* thickness). For mapping motor areas, the tasks were self paced done at each subject's comfort level.

The fMRI activations were recorded for hand, foot, and lip motor areas. Irrespective of the task paradigm four task epochs of 30 second duration were interleaved with three 10 second rest epochs for all the three motor tasks. SPM2 was used for reconstruction of the fMRI. The fMRI was subsequently aligned with the anatomical high resolution 3D-SPGR, and the baseline DWI scan.

3. Results

In this section, we show the results of comparing the developed two-tensor tractography method to traditional single tensor tractography and a probabilistic tractography method when applied to both simulated and in-vivo brain data.

3.1. Simulated Data

A simulated data set of crossing fibers was created to compare the performance of the algorithm tracing through the crossing area. Fig. 1a shows a slice through the data set in which the fibers cross at a 60° angle. The region in the middle of the image (shown in brown) is where the fibers cross each other. Fig. 1b illustrates the fiber tracts reconstructed from standard single tensor tractography. The tractography method was seeded in a region that can be best described by the single tensor fit. One would expect the fibers to continue horizontally; instead as they approach the crossing region the fiber tracts diverge in the wrong direction. Fig. 1c illustrates the connection probability map as a result of probabilistic tractography. The result shows that the estimated pathways have leaked and are dispersed, which makes the main connectivity paths more difficult to comprehend. Fig. 1d illustrates the fiber tracts obtained from the XST method. The fibers cross straight through, correctly following the horizontal fiber direction through the fiber-crossing region. Moreover the method is robust despite of the low SNR, however, the sensitivity of the method to different noise levels is not the focus of this study.

In summary, Fig.1 shows that single tensor deterministic tractography (Fig. 1b) results in erroneous tracts, probabilistic tractography (Fig. 1c) results in too many tracts (i.e. the visualization is hard to comprehend),

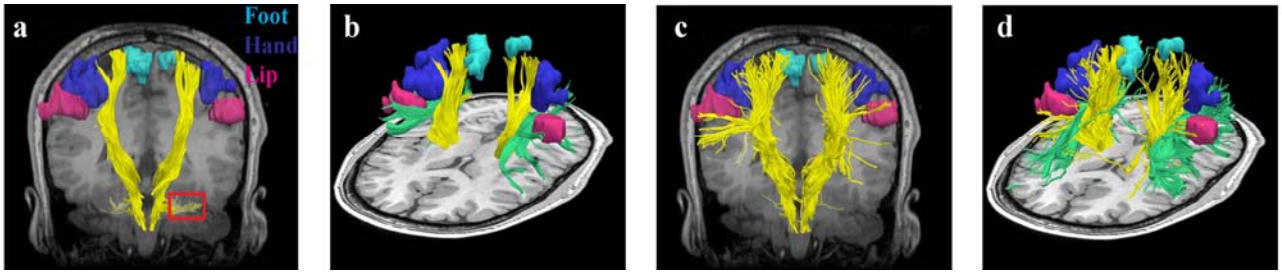

Figure 2: Single tensor vs. XST when seeded in the internal capsule. The fibers from the motor tracts are shown in yellow. (a) Fibers from single tensor tractography overlaid on the FMRI activation areas. Note that fibers in the cerebellum (region marked in red) behave erroneously by diverging laterally. (b) Fibers in (a) shown laterally. Additionally fibers from the SLF (green) are also shown. (c) Fibers from XST. The fibers are able to reach the fMRI activation areas. (d) Fibers in (c) shown laterally.

while XST (Fig. 1d) is able to trace the two individual tracts through the crossing area, without dispersing or terminate early.

3.2. In-Vivo Fiber Tractography

Fig. 2 shows the single tensor and two tensor tractography results overlaid on the fMRI activation areas in one subject. Fig. 2b,d also show fibers from the SLF, crossing the motor fibers.

The different tractography methods were seeded in the posterior limb of the internal capsule with a manually drawn region of interest. Fig. 2a,b shows the trace-lines as reconstructed by single tensor tractography. Fig. 2a,b shows that single tensor tractography can only depict part of the motor fibers (running superior-inferior): the hand and the lip fibers are not detected at all. Additionally Fig. 2a shows that the fibers in the cerebellum (Pontine fibers) behave erroneously by diverging laterally. In contrast Fig. 2c,d shows that XST is able to reconstruct fibers that are able to propagate to the different motor areas.

The probabilistic tractography results in a connection map that indicates the confidence level of a certain path. To be able to have a fair comparison (to probabilistic tractography) we generated maximum intensity projection (MIP) maps of single and XST based tractography. Fig. 3 illustrates these maps. Probabilistic tractography methods can in principle trace through regions of crossing fibers, but Fig. 3c shows that in this example the method fails to depict the fibers in the hand and lip areas. The figure depicts widespread dispersion but nevertheless, the majority of the streamlines (shown in yellow) fail to reconstruct the connections to the hand and lip fMRI activations.

The probabilistic method utilizes a model to generate a probability distribution function describing the distribution of fiber orientations at a given point in the brain. In fact most of the probabilistic methods rely on an underlying model of diffusion that helps in inferring the fiber orientation information. The underlying model may not be robust enough to accurately describe the underlying diffusion function. Our method utilizes a model that along with a mathematical framework has physical underpinnings. The underlying diffusion model has a large impact in tractography regardless of whether the method is deterministic or probabilistic, so choosing a better model may also improve probabilistic tractography results. Irrespective of the model, however, probabilistic tractography will likely disperse (as in Fig. 1c and Fig. 3c). In contrast, Fig. 1d, Fig. 2c,d, and Fig. 3d show that deterministic tractography yields a solution that is easier to comprehend, and at the same time can be carried out in real time.

In terms of computational time efficiency XST took approximately 1s to generate a single trajectory from a seed point. In contrast, the probabilistic tractography was a two-step process. A pre-processing step which involved generating various parameters required for tractography, and was computed once for each subject. This step took approximately 48h, after which the next step of trajectory generation (based on a seed point) took approximately 10s. Both methods were tested on a Pentium 4 processor, with 4GB of RAM.

4. Discussion

In this study we evaluated whether multi-tensor tractography can be used to visualize fiber tracts in areas of multidirectional fiber architecture in the brain. Such areas have proven to create problems for single tensor tractography method. An example of such an area is in the centrum semiovale. The reason that traditional tractography fails in regions where multiple fiber bundles (the motor fibers, and fibers from superior longitudinal fasciculus) intersect is that the Gaussian single tensor model cannot describe this complexity. As highlighted in this paper, areas of multidirectional diffusion are not only present in rare isolated regions, but also in the major clinically important fiber tracts. For example, the correct depiction of motor pathways (specifically that course laterally to the hand and face areas) is clinically critical for neurosurgical planning. The fiber crossing problem has

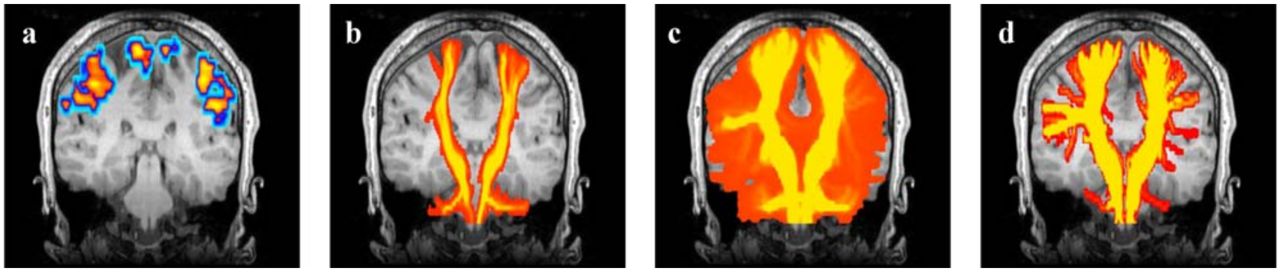

Figure 3: Tracing the motor tract when seeded from the posterior limb of the internal capsule. To have a similar visualization for comparison (to probabilistic tractography) a coronal maximum intensity projection map is shown. (a) The FMRI activation areas. (b) Single tensor tractography, voxels are color coded based on the number of trajectories passing through them. (c) Probabilistic tractography. (d) XST. In (b), (c), and (d) the colored regions show voxels containing at least one fiber trajectory.

been shown to affect single-tensor based streamline motor tract tracing for neurosurgery [20, 21]. In this paper we have shown that results from a multi-tensor tractography method can visualize motor fibers that could not be seen in the results from single-tensor tractography.

A criticism for deterministic tractography is the lack of a measure describing confidence or uncertainty of the reconstructed trajectories. This may be a reason for the recent interest in probabilistic tractography techniques, since with those methods it is possible to quantify the degree of uncertainty in the principal diffusion direction. For regions where there is a single dominant fiber pathway (such as the corpus callosum), the uncertainty in the principal diffusion direction is very small, therefore you would expect minimum dispersion in the connectivity maps from probabilistic tractography. However the dispersed behavior of tracts shown in Fig. 1c as a result of seeding in a single tensor region (mimicking the corpus callosum) is not what the clinicians are looking for. The aim of any tractography algorithm is to obtain reconstruct tracts that accurately correlates with the underlying white matter pathways. Given a 3D volume of connectivity maps with a dense map of frequent visitations it is extremely difficult to pick the most probable path. In short, clinicians such as neurosurgeons want to know where the fiber pathways are located, not where they might be probable. Additionally, the connectivity maps from probabilistic tractography fail to indicate the reproducibility of a certain path (given the samples of data). These maps are no more than an indicator of the number of visitations that a certain path underwent (from the seed point). If the underlying data is erroneous then a high connectivity index between two points does not guarantee an underlying white matter pathway. Therefore, as a result probabilistic tractography algorithms may also suffer from the problems arising from noisy data.

A limitation of our study is that the sensitivity of the results regarding parameter selection (such as C_p, radius of curvature, and ROI for seeding) has not been thoroughly studied. With a different choice of parameters, such as denser seeding we could reconstruct a larger number of trace-lines in, for example, the motor cortex. The use of C_p as a criterion for classifying voxels with crossing fiber tracts is a simplification and more complex models can be considered. Previous works have used statistical methods such as an F-Test to decide whether it makes sense to fit a more complex model when the simpler model is enough to describe the data [22]. Our initial experiments with information criterion methods [23, 24] for model selection were not very promising. This might be because Peled et al's [9] two-tensor model is constrained and comparing that to an unconstrained single tensor model might not be feasible. When evaluating the model selection criterion we need to formulate the inclusion of these constraints, which might not be trivial.

Future work will involve a qualitative study on the behavior of the different parameters for XST based tractography, along with evaluation of the technique on more subjects, and development of a more robust criterion (to either replace or complement C_p) for quantification of goodness of fit of the underlying model. It would be interesting to carry out a comparison study of probabilistic tractography based on different models of diffusion, such as the model proposed in [9].

5. Conclusion

Two-tensor deterministic tractography shows promise in resolving trace-lines in areas of crossing fibers. We have shown that using two-tensor streamline tractography method, it is possible to visualize white matter fiber tracts that are obtainable using single tensor tractography approaches. Although probabilistic tractography results perform better than single tensor stream-line tractography results, they show more dispersion than the results obtained using the presented two-tensor method. This dispersion describes uncertainty in the tractography results, and quantification of this may be important in some applications, however, this dispersion is undesirable for application domains such as neurosurgical planning. By reconstructing fiber bundles in the motor cortex and using fMRI activations we were able to assess that our approach could track hand, foot, and lip fibers of the corticospinal tract.

Acknowledgements: Supported by NIH P41-RR13218 (NAC), R01-MH074794, U41-RR019703, and the Brain Science Foundation.

References

[1] P. J. Basser, S. Pajevic, C. Pierpaoli, J. Duda, and A. Aldroubi, "In vivo fiber tractography using DT-MRI data," *Magnetic Resonance in Medicine*, vol. 44, pp. 625-632, 2000.

[2] T. E. Conturo, N. F. Lori, T. S. Cull, E. Akbudak, A. Z. Snyder, J. S. Shimony, R. C. McKinstry, H. Burton, and M. E. Raichle, "Tracking neuronal fiber pathways in the living human brain," *Proceedings of the National Academy of Sciences*, vol. 96, pp. 10422-10427, 1999.

[3] A. L. Alexander, K. M. Hasan, M. Lazar, J. S. Tsuruda, and D. L. Parker, "Analysis of partial volume effects in diffusion-tensor MRI," *Magnetic Resonance in Medicine*, vol. 45, pp. 770-780, 2001.

[4] E. O. Stejskal and J. E. Tanner, "Spin Diffusion Measurements: Spin Echoes in the Presence of a Time-Dependent Field Gradient," *Journal of Chemical Physics*, vol. 42, pp. 288-292, 1965.

[5] P. T. Callaghan, C. D. Eccles, and Y. Xia, "NMR microscopy of dynamic displacements: k-space and q-space imaging," *Journal of Physics [E]*, vol. 21, pp. 820-826, 1988.

[6] R. T. Tuch DS, Wiegell MR, Wedeen VJ, "Diffusion MRI of complex neural architecture," *Neuron*, vol. 40, pp. 885-895, 2003.

[7] D. C. Alexander, "Multiple-Fiber Reconstruction Algorithms for Diffusion MRI " *Annals of the New York Academy of Sciences*, vol. 1046, pp. 113-133, 2005.

[8] R. Blyth, P. Cook, and D. C. Alexander, "Tractography with multiple fibre directions," in *Annual Meeting of the International Society for Magnetic Resonance in Medicine*, 2003, p. 240.

[9] S. Peled, O. Friman, F. Jolesz, and C.-F. Westin, "Geometrically constrained two-tensor model for crossing tracts in DWI," *Magnetic Resonance Imaging*, vol. 24, pp. 1263-1270, 2006.

[10] R. Deriche and M. Descoteaux, "Splitting tracking through crossing fibers: multidirectional Q-ball imaging," in *IEEE International Symposium on Biomedical Imaging: From Nano to Macro (ISBI'07)*, 2007.

[11] G. J. Parker and D. C. Alexander, "Probabilistic Monte Carlo based mapping of cerebral connections utilising whole-brain crossing fibre information," *Information Processing in Medical Imaging*, vol. 18, pp. 684-695, 2003.

[12] T. E. Behrens, H. J. Berg, S. Jbabdi, M. F. Rushworth, and M. W. Woolrich, "Probabilistic diffusion tractography with multiple fibre orientations: What can we gain? ," *Neuroimage*, vol. 34, pp. 144-155, 2007.

[13] P. Staempfli, T. Jaermann, G. R. Crelier, S. Kollias, A. Valavanis, and P. Boesiger, "Resolving fiber crossing using advanced fast marching tractography based on diffusion tensor imaging," *Neuroimage*, vol. 30, pp. 110-120, 2006.

[14] P. J. Basser, "Inferring microstructural features and the physiological state of tissues from diffusion-weighted images," *NMR in Biomedicine*, vol. 8, pp. 333-344, 1995.

[15] D. LeBihan, E. Breton, D. Lallemand, P. Grenier, E. Cabanis, and M. Laval-Jeantet, "MR imaging of intravoxel incoherent motions: application to diffusion and perfusion in neurologic disorders," *Radiology*, vol. 161, pp. 401-407, 1986.

[16] M. E. Bastin, P. A. Armitage, and I. Marshall, "A theoretical study of the effect of experimental noise on the measurement of anisotropy in diffusion imaging," *Magnetic Resonance Imaging*, vol. 16, pp. 773-785, 1998.

[17] C.-F. Westin, S. E. Maier, H. Mamata, A. Nabavi, F. A. Jolesz, and R. Kikinis, "Processing and visualization for diffusion tensor MRI," *Medical Image Analysis*, vol. 6, pp. 93-108, 2002.

[18] S. Pajevic, A. Aldroubi, and P. J. Basser, "A continuous tensor field approximation of discrete DT-MRI data for extracting microstructural and architectural features of tissue," *Journal of magnetic resonance*, vol. 154, pp. 85-100, 2002.

[19] C. Pierpaoli, P. Jezzard, P. J. Basser, A. Barnett, and G. Di Chiro, "Diffusion tensor MR imaging of the human brain," *Radiology*, vol. 201, pp. 637-648, 1996.

[20] M. Kinoshita, K. Yamada, N. Hashimoto, A. Kato, S. Izumoto, T. Baba, M. Maruno, T. Nishimura, and T. Yoshimine, "Fiber-tracking does not accurately estimate size of fiber bundle in pathological condition: initial neurosurgical experience using neuronavigation and subcortical white matter stimulation," *Neuroimage*, vol. 25, pp. 424-429, 2005.

[21] N. Mikuni, T. Okada, N. Nishida, J. Taki, R. Enatsu, A. Ikeda, Y. Miki, T. Hanakawa, H. Fukuyama, and

N. Hashimoto, "Comparison between motor evoked potential recording and fiber tracking for estimating pyramidal tracts near brain tumors," *Journal of Neurosurgery*, vol. 106, pp. 128-133, 2007

[22] D. C. Alexander, G. J. Barker, and S. R. Arridge, "Detection and modeling of non-Gaussian apparent diffusion coefficient profiles in human brain data," *Magnetic Resonance in Medicine*, vol. 48, pp. 331-340, 2002.

[23] H. Akaike, "A new look at the statistical model identification," *IEEE Transactions on Automatic Control*, vol. 19, pp. 716-723, 1974.

[24] G. Schwarz, "Estimating the dimension of a model," *Annals of Statistics* vol. 6, pp. 461-464, 1978.